21

The Development of Concepts in Light-Emitting Devices

Claude Weisbuch

Departement de Physique et Laboratoire de Physique de la Matière Condensée,

Ecole Polytechnique, 91128 Palaiseau France

In these lecture notes we introduce the various physical concepts which have been put to good use in the past 30 years since the invention of the semiconductor laser diode. We then evaluate the various advances which led to the modern quantum well laser, including the use of strain effects and quantum barriers. Semiconductor lasers are nowadays fabricated and used in a wide range of realizations. We give a number of recent illustrations such as high-power arrays, high-speed lasers, short and long wavelengths lasers etc... To obtain still better light-emitters one needs to obtain sharp optical features and enhanced light-matter interaction in solids. We describe the recent advances in lower dimensionality quantized systems such as 1D quantum well wires and OD quantum dots. While most of the effort has been, and still is, devoted to the quantization of electron motion in low-dimensional structures, a new promising scheme has recently appeared based on photon mode quantization in optical microcavities, photonic bandgap materials and other photon localization structures. It leads to many features similar to those obtained by electron motion quantization, such as sharp emission lines, but also to several better ones: directionality, "thresholdless" lasers, strong light-matter coupling etc... Finally, we compare the two schemes of electron or photon confinement and show that the difference in potential performance is based on the Fermion or Boson nature of the particles.

I. Introduction

Light emission processes are today at the root of a large industry. Whereas the pace of progress has been uninterrupted since the beginnings, and some of the needs are well satisfied or on the verge of being so, others are not, most often due to some fundamental reasons.

Lasers show continuous progress towards lower threshold current, higher conversion efficiency (already in many cases above 50%), higher modulation rates, lower noise, higher operating temperatures, new wavelength ranges... In that field, it seems that the concepts needed to reach better performance are already here and that what is further required is better implementation of the concepts through better materials, technological fabrication processes, more clever structures etc...

On the other hand, light-emitting diodes (LEDs) are progressing at a much slower pace, although the commercial market is larger than that of lasers. This is because beyond the steady progress of light-emitting materials in improved internal quantum efficiencies, wavelength ranges, even chemical nature (see e.g. the recent breakthroughs in high- efficiency light-emitting polymers) the external quantum efficiency is limited by the poor extraction efficiency of light from an high-refractive index material into air[1]. For our purpose here it suffices to remark that, without photon recycling, a single planar semiconductor LED has an outside quantum efficiency of $\approx$ 3 - 4 % due to the poor extraction efficiency. This ridiculously low value presents a major challenge to the physicist, the more so if one tries to beat this "natural" factor with a planar, mass-production compatible structure. A strong effort in this field is certainly of major interest if one recalls the relative market sizes of light-emission devices: in Japan in 1993, the laser market was US $475 millions, the LED market was US $755 millions, the LCD display market was US $2.5 billions, the CRT market being still larger.

In view of these figures, it is all the more astonishing that physicists have so far devoted so little efforts to improve the optical performance of LEDs and electro-luminescent displays. This might well be due to the fact that the laser appears much more appealing to physicists due to its larger contents of physical concepts. As we shall see below, many new concepts can be put to good use to improve the LED efficiency beyond its natural value, which is however being presently improved by the use of 3D structuring on mirrors[1,2].

The major field which escapes solid-state devices is that of displays, which are so far mainly based on cathode-ray tubes (CRTs), and partly on liquid crystal displays (LCDs) in their flat form or embedded in projection systems. Electroluminescent (EL) or plasma displays play a very minor role. Addressing the needs of the display industry therefore represents another major challenge to semiconductor device physicists who have to solve several issues if they are to succeed in displacing competing technologies somewhat less "elegant" in terms of physics, but certainly very "efficient" in terms of satisfying the needs of a very wide-scale industry, with a lot of potential growth due to the replacement needs of an installed base of more than one billion TV sets, to the increasing the pervasiveness of images in our everyday life, to the overall world economic development.

So far, the effort towards better light-emitting devices has been two-fold. The first line of action has been devoted to reaching intrinsic light-emission mechanisms, i.e. reducing non-radiative extrinsic or intrinsic processes, degradation mechanisms, improving injection or excitation efficiencies... Quite often such improvements have been described by quantum efficiency factors improving towards unity. We will essentially not discuss this effort, in spite of its importance. The second line of action, not always conscious, has been towards the improvement of the intrinsic emission parameters by the controlled design of the electron and electromagnetic degrees of freedom. This is well illustrated by the various concepts developped along the years which have led to the diminishing of the threshold current of semiconductor lasers, as shown in Fig. 1. As can be seen there, we are entering a fourth generation of semiconductor laser concepts, which through continuous modeling and material improvement led to threshold current densities in the few tens of A cm^{-2}

range starting from 10^5 A cm^{-2} ! The first major breakthrough was brought by the use of double-heterostructures around 1970 (the second generation of devices), which allowed continuous operation of laser diodes by the reduction of the threshold current in the kA/cm^2 range. The 1980's saw the impact of the new fabrication techniques of MBE and MOCVD through the use of two-dimensional (2D) quantum wells as active materials layers (third generation). Finally, the fourth generation of semiconductor lasers is in the making, induced by the search for full electron or photon quantization, and their device applications[3,4].
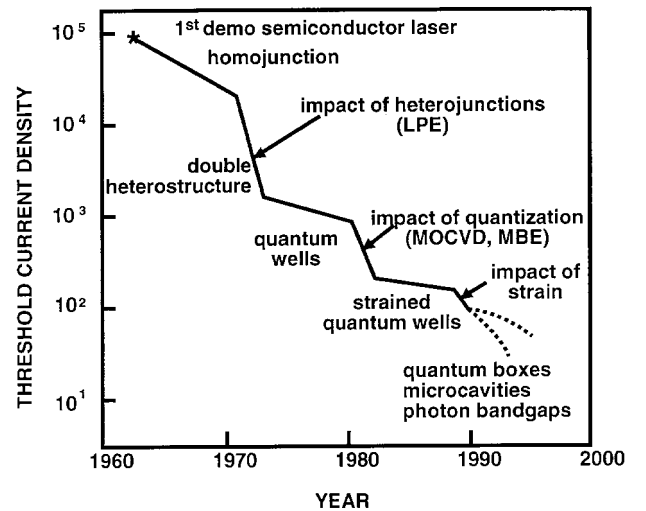

Figure 1. Evolution of semiconductor laser current threshold.

In this tutorial paper, we will briefly describe the various phases leading to quantum well laser in its various forms, and then discuss the more open concepts of electron quantization in quantum wires and dots, or photon mode quantization in microcavities or photonic bandgap materials.

II. The semiconductor laser from the simple p-n junction to the present-day quantum well laser

II.1 The laser building blocks

II.1.1 Threshold equation

Fig. 2 shows the schematics of a semiconductor laser. Emission takes place between two mirrors (simply cleaved semiconductor-air interfaces in the case of Fig. 2a). For an optical wave which is an eigenmode
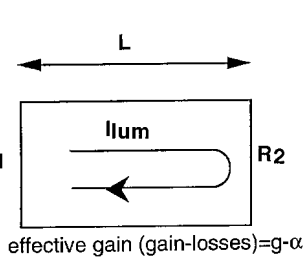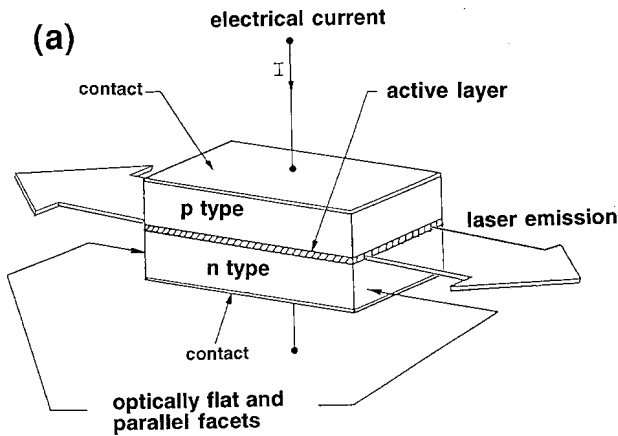
of the cavity (i.e. verifying $2kL = 2n\pi$, the phase condition), the threshold condition is obtained by stating that the intensity is unchanged after a round-trip in the cavity

$$R_1 R_2 e^{(g-\alpha)2L} = 1 \tag{1}$$

where R_1 and R_2 are the reflexion coefficient of the mirrors (≈ 0.3 in the case of cleaved faces, see below), g is the gain, α represent the losses of the optical wave due to the carrier absorption, light scattering due to waveguide imperfections... The gain at threshold then reads

$$g = \alpha + \frac{1}{2L} Log \frac{1}{R_1 R_2} \tag{2}$$

With typical numbers $R_1 = R_2 = 0.3$, $L = 250 \mu$m, $\alpha = 10$ cm^{-1}, the threshold gain is 50 cm^{-1}.

(a)

electrical current

contact —   active layer

p type

n type

laser emission

contact

optically flat and parallel facets

(b)

L

R1   Ilum   R2

effective gain (gain-losses)=g-α

Threshold condition roundtrip balance

$$I_{lum} e^{(g-\alpha)2L} R_1 R_2 = I_{lum}$$

Figure 2. (a) schematics of a semiconductor laser (b) balance equation for an optical wave undergoing a rountrip in the cavity.
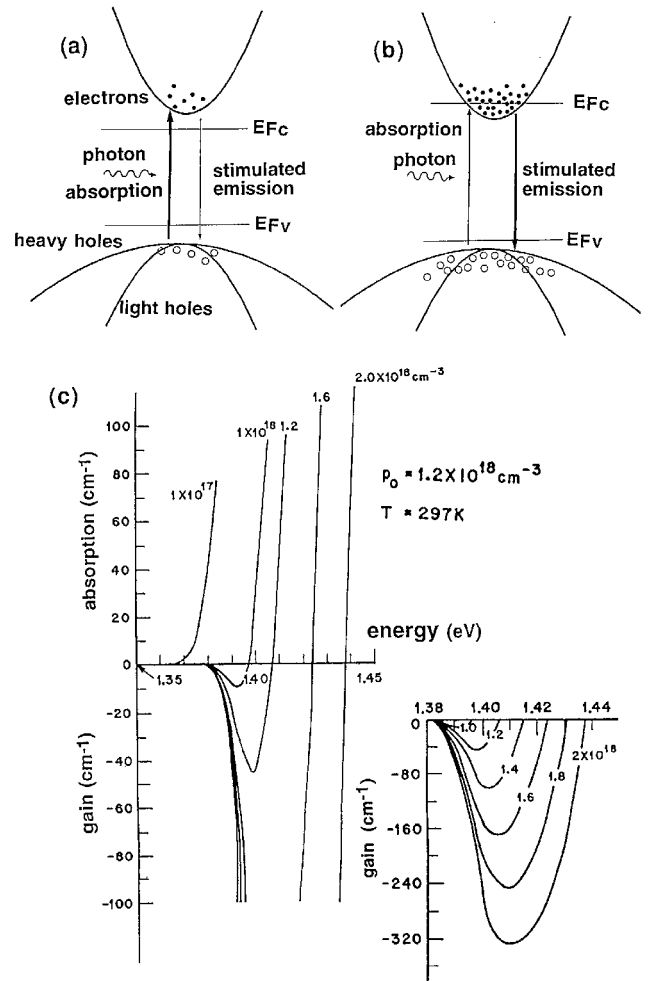

Figure 3. Schematics of gain formation in a semiconductor: (a) and (b) absorption and stimulated emission transitions under weak (a) and strong (b) injection; Note the position of the quasi-Fermi levels E_{F_c} and E_{F_v}; (c) absorption and gain under increasing excitation (from Casey and Panish[6]).

Fig. 3 schematically depicts the formation of gain in a semiconductor structure. Under electrical injection of electrons and holes in the active region from n and p adjacent regions, one creates an inversion of population near the band edge. Inversion is reached when the stimulated emission induced by an incoming photon is larger than its absorption coefficient. The equality regime is called the transparency of the active medium. As the Einstein coefficients describing these two events are equal, the inversion condition is only determined by the occupancy factors f_c and f_v of the conduction and valence bands respectively, through

$$f_c(1 - f_v) > f_v(1 - f_c) \tag{3}$$

Using the quasi Fermi levels E_{F_c} and E_{F_v} to express

the occupancy factors, (3) becomes

$$E_{F_c} - E_{Fv} > h\nu \qquad (4)$$

the well-known Bernard-Durrafourg equation which shows that at least one quasi- Fermi level must penetrate one of the bands (conduction or valence) as the emitted photon energy hv is at least the bandgap energy E_g.

Through electrical injection, the carrier densities are equal, which expressed in terms of the equivalent densities of states N_c and N_v of the bands approximatively yields

$$N_c f_c = N_v f_v \qquad (5)$$

From there, it is easy to see that if N_c and N_v are equal, $f_e = f_h = 0.5$ satisfies (3). However, in III-V materials $N_c \approx 0.25 N_v$. Therefore one needs a much higher occupancy factor in the lower density band, here the conduction band, to satisfy (3). Indeed, to satisfy both (3) and (5) one requires $f_c \approx 0.8$ and $f_v = 0.2$. Due to the asymmetry between the bands electron band filling needs to be quite increased compared to a symmetric situation. This is presently solved by the use of strained quantum wells which symetrize the valence band with respect to the conduction band by splitting away the various hole sublevels and by changing the dispersion of holes to light-hole like.

Once inversion is reached, additional carriers create net gain. The standard calculation requires to sum over the various transitions which can occur between all electron-hole pairs, inverted or not. The former give gain, the latter absorption. A simpler model considers the electron-hole pair system as a two-level system with an homogeneous linewidth $\Delta\nu$ given by the occupancy factor of carrier states, i.e. kT/h. Then, the gain is given by the standard formula[5]

$$g \simeq \Delta n \frac{c^2}{8\pi\nu^2 n_{opt}^2 \tau_{sp}} \frac{1}{\Delta\nu} \qquad (6)$$

where Δn is the excess density above the inversion density (or transparency density) n_0

$$\Delta n = n - n_0 \qquad (7)$$

and τ_{sp} the spontaneous radiative lifetime (which contains the optical matrix element). From formula (6) with $\tau_{sp} \approx 3.10^{-9}$s, one finds that for $g = 50$ cm^{-1} $\Delta n \approx 0.4 \quad 10^{17}$ cm^{-3}. This is within a factor of 5 of what is measured and calculated in the full manner[5] (Fig. 3c), which is not surprising considering the many simplifying assumptions contained in equation (6) (isotropic emission, single emitting level, simple kT broadening...). Using the Casey-Panish value $\Delta n = 2.10^{17}$cm^{-3} and $n_0 \approx 10^{18}$ cm^{-3}, the threshold carrier density is 1.2 $\quad 10^{18}$ cm^{-3}.

II.1.3 Optical confinement factor

An additional parameter is required in equation (2), the optical confinement factor Γ which represents the fraction of the optical mode of the laser which overlaps with the active region with gain. It is indeed only that fraction Γ of the wave that is able to create stimulated emission. However, it is the whole of the optical wave which undergoes losses. Then, equation (2) becomes

$$\Gamma g = \alpha + \frac{1}{2L} Log \frac{1}{R_1 R_2} \qquad (8)$$

How much is L ? In the original p-n junction laser, the optical wave width is of the same order of magnitude as the carrier diffusion length, in the micron range. Therefore, the overlap is nearly unity. For double-heterostructures (Fig. 4) carriers are confined within the central active layer by the potential barriers existing at the hetero-interfaces. The optical wave is guided by the higher index of refraction of the active, smaller-bandgap material[6]. This waveguiding effect is effective down to an active layer thickness of 0.1 μm, for which the optical confinement factor is still ≈ 1. Below such thickness, the active laser is too thin to have a strong waveguiding effect. This is exactly similar to the poor electron confinement in thin quantum wells when the electron confining energy is comparable to the well energy depth and when the electron wavefunction penetrates deeply in the barrier material. In the optical waveguiding context, the optical wave becomes wider linearly with decreasing active layer thickness, which leads to a decreasing optical confinement factor varying

as d^2, due to the concurrent decreasing overlap factor of an increasingly wide optical mode with a narrower active layer. An approximate value is[6]

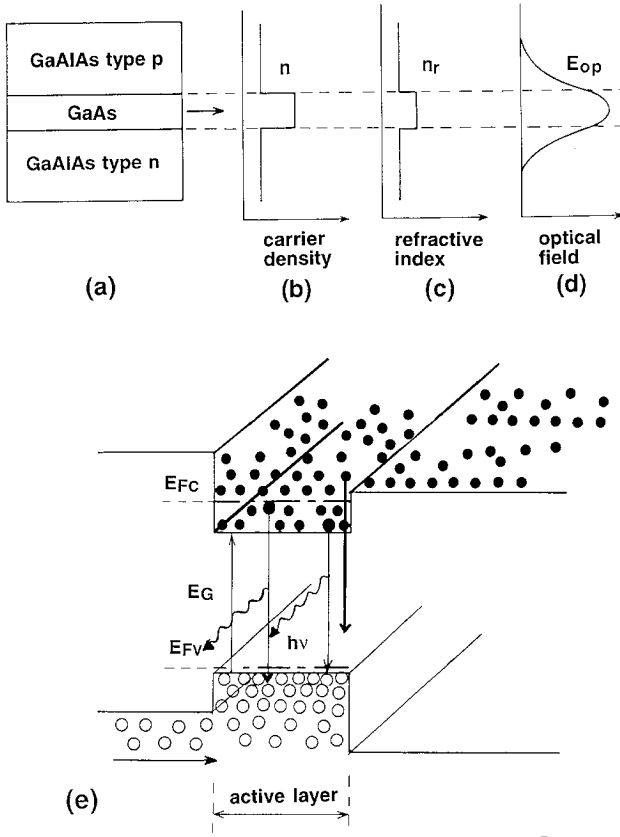$$L \approx 2\pi^2 (n_2^2 - n_1^2) d^2 / \lambda_0^2 \qquad (9)$$

Figure 4. Schematics of a double heterostructure laser (a), showing carrier density (b), refractive index (c), optical waveguiding (d), and spatial distribution of carriers (e).

II.1.4 Mirrors

As shown on Fig. 2a mirrors are often made of cleaved interfaces, with a reflexion coefficient given by

$$R = \left(\frac{n_2 - n_1}{n_2 + n_1} \right)^2 \qquad (10)$$

which for $n_2 \approx 3.3$ and $n_1 = 1$ give $R \approx 0.3$. Very often, the laser facets are coated, either for protection (mainly passivation against oxyde formation), or for the selection of one facet as an output facet by coating the other one with an high R multilayer reflector, or for diminishing the threshold current by diminishing the mirror loss in equations (2) and (8).

In the planar geometry of so-called Fabry-Perot lasers (Fig. 2a) one is able to obtain reflectivity coefficients up to 0.9 reasonably easily. Higher values are difficult to obtain reliably because of the inconvenient geometry for mirror deposition.

For a number of applications, in particular vertical-cavity surface emission lasers (VCSELs), one needs higher reflectivity mirrors. Although they have large absorption losses, metals are sometimes used in hybrid mirrors which also play the role of electrical contacts. The most widely used solution consists of multilayer stacks of quarter-wave dielectrics which realize Bragg mirrors[7]. The optical wave amplitudes reflected at each interface add constructively in phase and one reaches reflexion coefficients above the 0.99 range with 20 GaAs/AlAs alternate pairs, with very low losses. Of course, materials pairs with high-index difference will require less periods as the reflection coefficient for each pair period will be higher. Of particularly interest is the recent advent of oxydized $GaAs/Al_xO_y$ mirrors which already led to high-efficiency LEDs and low-threshold lasers[9].

II.2. The progress towards present-day lasers

Using the above building blocks we can describe the various effects leading to the performance of actual quantum well lasers.

The junction laser required to create $1.6 \ 10^{18}$ carriers per cm^3 in the active volume to reach threshold (the loss factor α is 100 cm^{-1} because the optical wave penetrates highly doped regions). With an excited thickness of 3 μm, this translates into $4.8 \ 10^{14}$ carriers per cm^2, and into a threshold current of $2.10^4/cm^2$ assuming $\tau \approx 3$ ns, using the relation

$$J_{th} = \frac{n^{3D} e d}{\tau} = \frac{n^{2D} e}{\tau} \qquad (11)$$

The double-heterostructure laser both confines the optical wave and carriers into an optimum thickness of 0.1 μm^5. Assuming a unit confinement factor for such a thickness, a threshold carrier density of $1.2 \ 10^{18} \ cm^{-3}$ is required to achieve the volume gain of 50 cm^{-1} required to satisfy eq. (8). This translates into a sheet carrier density of $1.2 \ 10^{13} \ cm^{-2}$ and a threshold current

density of 640 A/cm^{-2}. The origin of the improvement when compared to the simple p-n function laser is obvious: the joint squeezing of carrier density and optical wave by the double-heterostructure allows to operate at the same gain and therefore constant injected volume carrier density. But by decreasing the volume in which such carrier density must be created one diminishes the current areal density.

The quantum well laser continues this trend. In their original patent Dingle and Henry mainly focused on the improvement in the gain which can be achieved by a given number of carriers Δn above inversion. Indeed, in the square constant density of states (DOS) of quantum wells, carriers create gain more efficiently than in the parabolic DOS of a 3D DH structure[10]. Actually, that effect comes into play but it is quite smaller than the effect of diminished carrier density to be injected to achieve inversion (Fig. 5), as due to the freezing of one degree of freedom in QWs the density of states is strongly diminished. This reduces the transparency density by a factor of ten, while the more efficient carriers above transparency due to the square DOS (see Fig. 5) improve **gain per carrier** by a factor of two. The average gain per carrier is otherwise unmodified as the optical matrix element is the same in 2D or in 3D.

There is however a difficulty in using QWs as active layers, due to the smallness of the optical confinement factor Γ (see eq. (9)). A first way to circumvent that difficulty has been to use multiple QW (MQW) active regions, but then the required transparency density is multiplied by the number of QWs. The only advantage of using QWs is then in other useful operating features such as the higher operating frequency due to the larger differential gain of QWs near transparency current (Fig. 6d) or the slower temperature dependence of the threshold current due to the existence of a square DOS up to high energies, meaning that relatively fewer excited states are thermally populated than in other structures (Fig. 6c).

The single QW laser emerged thanks to a breakthrough imagined by Tsang[10], the use of separate-

confinement heterostructures (SCH). They beat the poor confinement factor given by formula (9) by separately confining photons in a wider optical cavity surrounding the active QW layer (Figs. 6a and 6b). Then, the optical wave is optimally- compressed in a 1000 Å-wide optical cavity, and a single quantum well typically 100 A thick yields a Γ of 0.1. This means that the volume gain required to reach threshold is 500 cm^{-1} (eq. (8)). This requires a volume density above transparency of 1   10^{17} (taking into account the factor of 2 improved gain per carrier due to the square 2D DOS), which is only 1   10^{11}cm^{-2} when translated into an areal density n^{2D}. As the transparency density is in the 10^{12} cm^{-2} range, this translates into threshold current density J_{th} of 110 A/cm^{-2}.

The values of the best of lasers are actually somewhat better than what has just been evaluated: several "second-order" effects have been neglected such as increased optical matrix elements by band selection (instead of the band averaging in the bulk), and also one should remember that the "record" structures for low-threshold operate at reduced optical losses (by using longer structures and reflecting mirrors). Also, the use of strain diminishes the transparency density (Table 1), so that the best reported values are in the range of 60 Å/cm^2 for GaInAs/GaAlAs structures (however with cavity length in the 800 μm range).

As can be seen, the progress between the DH laser and the QW laser is mainly due to the improvement in transparency current (Fig. 6d). It is so because it should be emphasized that semiconductor lasers with a 3D electronic structure are quite bad considering the principles of operation: one has to invert much more quantum states than those required above inversion to achieve laser gain. In other words, the 3D DH laser has many more quantum states than required to reach the threshold gain. In contrast, the QW laser just matches the number of quantum states to what is needed to achieve the required gain. This is all the more evident if one recalls the price to pay for such an optimization: due to the square DOS in 2D, the gain curve saturates at high injection (see Figs. 5 and 6d) and it could well happen that the maximum gain for one fully-inverted quantum state in a quantum well is not enough to reach
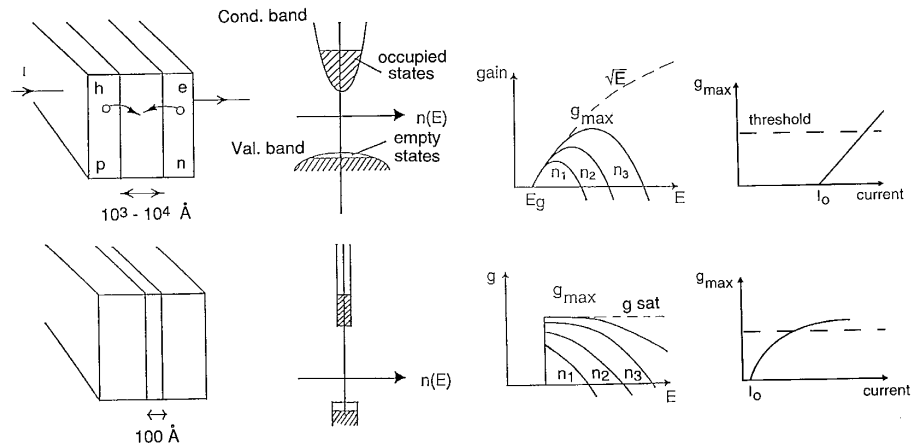
Figure 5: Schematics of the gain formation in 3D bulk DH active material (top) and in a 2D QW material (bottom). Due to the smaller density of states in 2D the transparency current I_0 is diminished. Due to the square density of states, a given number of injected carriers is more efficient to create gain in the 2D QW, which translates into a steeper gain-current curve.

threshold. This is usually not the case, as the gain per state is enough to reach threshold in usual structures. When a high-loss structure is used (short-cavity lasers), then lasing can only occur if additional gain can be obtained by filling an excited state[12] (gain increase indicated as E_{e2} on Fig. 6d).

From the above discussion, it is clear that the QW laser, having its performance based on the freezing of one degree of freedom and on the square 2D DOS, **is a truly 2-dimensional quantum device.**

II.3 The variety of quantum well lasers

In order to fulfill the various needs various structures and materials are being used:

1. If one searches for a low threshold current density one then operates with a single QW laser to minimize the transparency current. Which is then the best among the two structures, GRIN-SCH or SCH (Figs. 6a and 6b) ? Under operating conditions, the quasi-Fermi level of electrons is so high that significant population of the optical confining layers occurs. Then, it is obvious that the GRIN-SCH structure is the best as the number of such useless carriers is minimized[11,12].

2. On the other hand if one requires a temperature insensitive threshold one should use the multiple quantum well (MQW) laser (Fig. 6c): a major part of the temperature sensitivity is due to the thermal tail of the occupancy factor. As the larger 3D DOS of continuum states is the farthest away from the lasing level in MQW lasers, it is the one which minimizes high-energy

thermal electrons. Of course the threshold current at low temperatures will not be optimum.

3. To obtain visible emission, several avenues have been tried: in the red-orange region, GaAlInAs materials give good results. One of the limiting factor is the electron overflow over the gap discontinuity of the hetero-interface on the p side, which leads to electron leakage and recombination outside the active layer. This is due to the unavailability of large enough bandgap discontinuities with these materials. An elegant solution to this carrier leakage is the use of an electron Bragg mirror as the confining layer on the p side of the heterojunction: by alternating layers with thicknesses a quarter of the electron wave, one can construct a forbidden gap for thermal electrons impinging from the active layer. Very significant improvement in threshold currents have been obtained in this way[13].

For blue-green spectral regions new materials have to be selected. The Zn-based wide-gap materials (ZnSSe, ZnMgSSe) have been used with great recent successes. The main issue there is the fast degradation of such lasers under operation. Another promising route is that of the III-V nitrides, for which excellent LEDs have been obtained in spite of extremely high dislocation densities ($10^{10} - 10^{11}$ cm^{-2}), but so far there has not been any report of lasing action there[14,15].

4. In infrared lasers in the 1.3 - 1.5 μm range QW laser operation is made difficult because of the strong free carrier absorption (inter-valence bands) and of the Auger effect in the GaInAsP materials which introduce
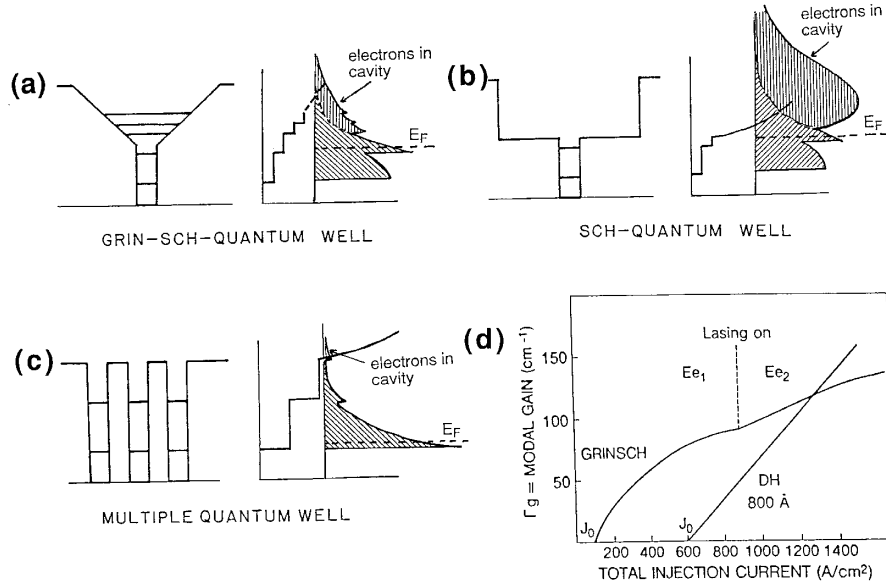
Figure 6. Quantum well laser structures and current-gain curves. (a): Graded-index separate confinement heterostructure laser (GRIN-SCH); (b): separate confinement heterostructure (SCH) single quantum well laser; (c) multiple quantum well (MQW) laser; (d) schematics of the gain-current curve for a single QW GRIN-SCH laser and a 800 Å active-layer DH laser. Note the large difference in transparency currents J_0, the curvature and saturation of the QW gain curve (due to the 2D DOS, see text) and a "desaturation" of the gain once an excited level (E_{e2}) starts to be populated.

Table 1 : Operating features of various types of semiconductor lasers

	Optical loss α cm^{-1}	Cavity loss $\frac{1}{2L}$Log$\frac{1}{R2}$ cm^{-1}	Transpar. density n_0 10^{18} cm^{-3}	Excess carrier density Δn 10^{18} cm^{-3}	Total carrier density 10^{18} cm^{-3}	Threshold density in active thickness d 10^{12}cm^{-2}	Threshold current density (τ=3ns) A/cm^2	Threshold current for 250µm ×2µm laser mA
p-n junction laser	100	40	1	0.6	1.6	480 (3µm)	2.6 10^4	130
DH laser	10	40	1	0.2	1.2	12 (0.1µm)	650	3.2
GRIN-SCH QW laser	10	40	1	1	2	2 (0.01 µm)	110	0.55
Strained GRIN-SCH QW laser	10	40	0.5	1	1.5	1.5 (0.01µm)	80	0.4

new loss mechanisms and carrier heating effects. Careful optimization of the confining layers and quantum wells is required to obtain laser emission[12].

5. Toward deeper IR emission (beyond 2µm) a variety of materials are being used: the In and Sb-based III-Vs (GaInAsSb), the Hg-based II-VIs(HgCdTe), the IV-VIs (PbSnSTe). Although reporting good efficiencies, all these materials suffer from rather delicate chemistry. The lasers in that energy range so far only operate at low temperatures due to the temperature-dependent loss mechanisms prevailing in these materials.

Very recently Capasso et al. have developed the Quantum-Cascade laser based on intersubband transitions[16]. These represent a very unique case of

unipolar laser. In order to achieve population inversion in such fast relaxing systems, a careful design has to be made. In particular electron Bragg mirrors are being used to prevent thermo-ionic emission from the upper laser level. Although such lasers are quite different from other interband lasers, the very general equation (6) describes quite well their operation.

6. High-power semiconductor lasers: Thanks to the lower transparency current QW lasers have a high electrical-to- optical quantum efficiency, often above 50%, while the differential quantum efficiency is above 90%. A double revolution is therefore under way, one about the ever increasing power of laser diode assemblies[17], the other about the broader use of such

high power diodes[18].

The increase in diode power requires the optimisation of laser structures for that application, efficient thermal coupling, improved reliability under high-current, high temperature operation. Without detailing the various aspects of this very fast developing area, let us just mention the continuous progress in mastering the facet reliability, by various types of protective measures[17]. Catastrophic optical damage (COD) usually due to the residual facet oxyde absorption limits the optical power density at 2.5 MW cm^{-2}, beyond which facet melting occurs. By using facet passivation layers, or better by burying the active material thanks to impurity-assisted interdiffusion, that threshold can reliably be raised up to 20 MW/cm^{-2}. Assemblies of laser diodes reach very high- powers, the present state-of-the-art being a 1 cm^2 stack of laser arrays emitting 1 kW in a quasi-CW manner.

II.4 Towards very low-threshold current laser

Typical active lasers have an intrinsic threshold current density of 100 A/cm^2. Reaching low threshold currents is then a matter of laser surface. A typical laser, 250 μm long and 2 μm wide, has a threshold current of 0.5 mA. In the same Fabry-Perot planar geometry, it is very difficult to diminish the laser width below 2 μm, as dif*active losses of the lateral rib waveguide become prohibitive (this is were photonic bandgap materials might play a big role - see below and J. Joannopoulos notes in this volume). The length can be diminished, but to retain the low threshold current density one needs to operate at constant optical loss. This requires to improve facet reflectivity. Using R=0.9 mirrors, a cavity length of 25 μm has the same optical loss of 40 cm^{-1} as the previous structure, thus the same threshold current **density**, but a threshold current of 50 μA, ten times lower. The present state-of-the-art in this geometry is in the 100 μA range.

To still diminish the laser surface one uses the vertical cavity geometry (Fig. 7b) with Bragg mirrors with $R > 0.995$. For an effective cavity length of 2 μm losses are 25 cm^{-1}. For a pillar with an 0.3 μm diameter, the transversal confinement factor would be unity but the longitudinal confinement factor is only about 0.5% per quantum well. To have enough gain one uses three

quantum wells. The threshold current density would then be typically 200 A/cm^2, which would give a threshold current of 0.2 μA. We are not yet there, but recent progress thanks to Al oxyde mirrors and lateral confinement lead to a threshold current of 8 μA with a pillar laser of 3 μm diameter[9].

Further progress could well make use of microdisk lasers[19] which have still lower optical losses, but for which useable outcoupling strongly reduces the outstanding intrinsic properties (fig. 7c).

III. Beyond quantum wells: quantizing electrons or photons?

In view of the successes of quantum well lasers, a first, obvious avenue to further progress is that of further structuring the material to obtain electron confinement in 1D quantum-well wires (QWWs) and OD quantum boxes (QBs). They however raise a major fabrication challenge: whereas the layered structure of 2D QWs is obtained in a natural 2D layer-by-layer growth mode, the structuration of QWWs and QBs clearly requires something more. The two main fabrication paths are that of etching materials (usually 2D QW structure) into lines or pillars[20], with difficulties associated with processing damage, and those relying on the direct organized growth. The latter have recently seen major advances and will be discussed below.

The second avenue, which recently opened in semiconductor microstructures, stems from newer concepts in quantum optics[21]. There, one tries to modify the atom- light interaction by controlling the photon modes with which atoms interacts. This is the field of cavity quantum electrodynamics[22] (CQED), for which the more recent concept of photonic bandgap (PBG) materials is a welcome addition[23−26]. The extension of the concepts of CQED to semiconductors has already yielded important results in fundamental or applied fields, and more are to come, due to the very important leverage (at the fundamental level) that photon mode control brings to the quantum optics "system designer".

The property which is being adressed in the two approaches of electron or photon confinement is that of the light-matter interaction. Under usual conditions, two continua of states interact with each other: the
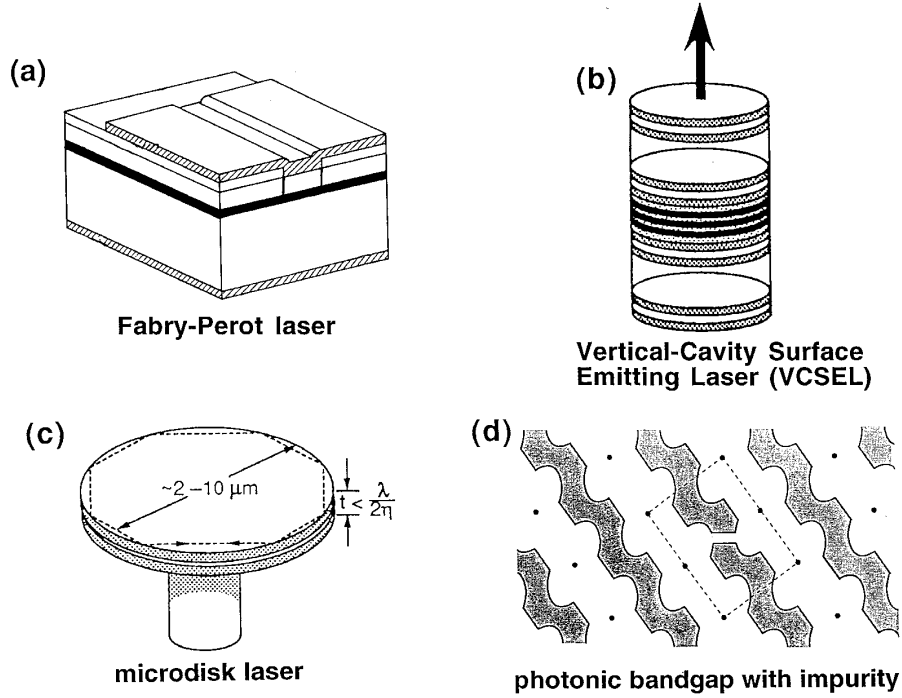
Figure 7. Schematics of four laser structures, three of them with "controlled" spontaneous emission. (a): standart Fabry-Perot laser; (b) vertical-cavity surface emitting laser (VCSEL); (c) microdisk laser; (d) photonic bandgap with impurity.

continuum of electron-hole states and the continuum of the energy-and momentum-matched photon states. This leads to the well-known thermally broadened optical features in solids, in particular those situated energetically near the fundamental band edge of semiconductors. Either confinement leads, through reduction in degrees of freedom, to sharper and sharper features as the optical transition rate, determined by Fermi's Golden rule, is the product of both the electron-hole and photon mode density-of-states (DOSs). Evidently, one obtains sharper and sharper features with more confined systems, i.e. going from 3D to 2D to 1D to 0D. The respective DOSs are shown in Fig. 8 for both types of confinement.

III.1. Confined Electron Structures:

III.1.1 Basic optical properties: sharper DOS, stronger exciton effects (?)

As the optical properties of 2D QW structures are by now quite-well documented, we will focus here on the properties of lD QWWs and 0D QBs, mainly stressing the newer points compared to 3D bulk semiconductors and 2D QWs.

1.   Optical   transitions   involving   **unbound electron-hole pairs** are characterized by an oscillator strength which is unchanged with dimensionality and therefore retains the 3D value f_{eh} **per transition**[3,4]. Therefore, diminishing dimensionality by diminishing the volume sharpens the DOS, but also reduces its energy-integrated absolute value by diminishing the number of quantum states. To retain a large light-matter interaction one requires to use a large number of QBs. Dealing with equal occupancy-integrated DOSs i.e. number of carriers, the advantage of concentrating the DOS in QBs is approximately given by the ratio of kT to the QB linewidth (Fig. 9). How much will that be? Recent photoluminescence have indeed evidenced the narrow linewidth ($\approx 10 \mu$eV) of single QBs, which unambiguously demonstrate the freezing of the translational degrees of freedom of the carriers. However the size fluctuations (see discussion below) seem to limit the inhomogeneous linewidth at best in the range 1-5 meV.

2. **Exciton effects** are modified when diminishing dimensionality. Takagahara has predicted that the exciton ls oscillator strength is further increased when com-
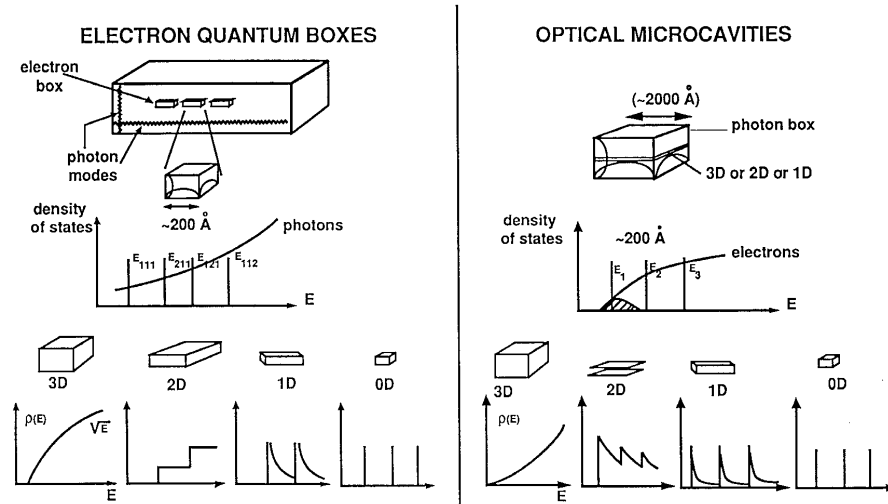
Figure 8. Schematics of quantization in electron quantum boxes or in optical microcavities.

pared to 2D QW excitons, at the expense of the oscillator strength of the unbound e-h pairs[27] (the so-called Sommerfeld factor). In OD, the situation depends on the QB size relative to the exciton radius, and one defines three regimes of confinement, weak, intermediate, strong corresponding to smaller and smaller QBs. In the weak confinement regime, the exciton motion is being quantized and if exciton quantization takes place (i.e. $L_{box} \lesssim$ exciton thermal wavelength) a "giant" oscillator strength can develop due to the coherence of the exciton wavefunction throughout the QB[27,28].

3. Any discussion about **device performance** must distinguish between those relying on **relaxed excitations** such as lasers, and those relying on **unrelaxed excitations**, such as electro-optic and nonlinear optical modulators. In the latter case, the properties of QWs in part rely on the excitonic nature of the absorption edge, even though it is somewhat broadened ($\simeq$ 5 meV) at room temperature. To obtain stronger features based on e-h pairs in QBs one would require, for QBs with an inhomogeneous width of 5 meV (quite difficult to achieve, see below), an areal density yielding an integrated oscillator strength equivalent to that of the QW exciton peak (i.e. 10^{12} cm^{-2}): this would mean QBs with center-to-center distances of the order of $\sim$200 Å. Even taking into account some of the increase in oscillator strength as described above, it ap-

pears quite difficult to increase the QB densities at the levels required to compete with QW exciton-based devices.

III.1.2. Application of QBs to lasers

The most sought-after device is the QWW or QB laser. The "intrinsic" improvement of QBs over QWs lasers is the $\sim$ 5 - 25 factor described above, due to the sharpening of the gain spectrum in QBs (Fig. 9). The much better threshold improvements predicted by some authors for QWW and QB lasers therefore originate in the smaller sizes of the QWW and QB lasers used in their comparisons with much larger QW lasers. For the sake of comparison, let us recall here that a typical QW laser has a current threshold of 0.5 mA. How much better would the QB laser be ? The gain of injected carrier being $\approx$ 5 - 25 times larger and forgetting the transparency current, the density would be diminished at best by a factor of 6 as the confinement factor Γ would be diminished by a factor 4, assuming a 50 % filling factor for each in-plane direction. However, in terms of number of carriers used to create the gain, the improvement is indeed a factor of 5 to 25 (the gain is created in the smaller volume of QBs as compared to QWs).

We will however see below that realistic evaluations of size fluctuations leave little hope to reduce the in-
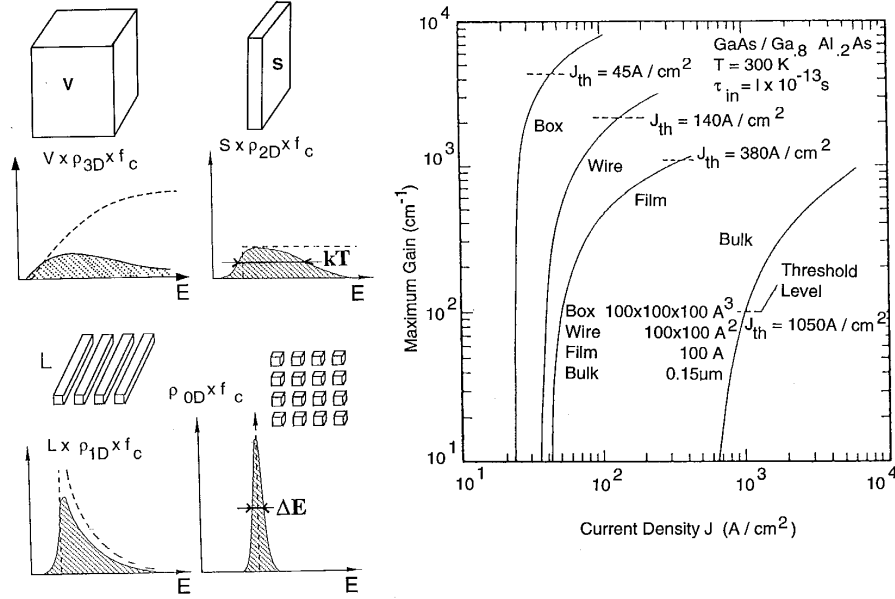
Figure 9. Comparison of gain formation in bulk QW, Quantum Wire (QWW) and Quantum Box (QB) materials, and corresponding gain-current curves (from Asada, 1986).

homogeneous linewidth below 5 meV. In that case, it means that the improvement will at best be a factor of 5 in the carrier density, translating into a required million QBs in our design laser of size 250μ m$\times 2\mu$m.

The large improvement in transparency current observed when changing from bulk DH active layer to QWs (discussed at length in paragraph II.2) does not occur again (see e.g. the various transparency currents in Fig. 9).

III.3. Issues in QB laser operation: size fluctuations, inhomogeneous broadening, relaxation bottleneck (?)

Beyond these simple scaling arguments, the operation of QWW and QB lasers rely on the implicit requirements that (i) the linewidth is narrower than that of thermally- broadened 2D and 3D systems and (ii) all excited carriers reach the ground state where they all participate in the gain. The first requirement can be straightforwardly evaluated: if we take cubic 100 Å GaAs QBs, a 5 meV linewidth requires a size fluctuation of $\approx$ 1 monolayer in all directions. The best fabrication techniques are still far from this, as is shown by the broad low-temperature photoluminescence spectra of multi-QB samples, while single QB experiments

give sharp-line spectra (Fig. 10). As mentioned above, an ultimate laser (2 μm$\times 0.3\mu$m$\times 0, 3\mu$m) would still require about 1000 QBs to operate. A 1 meV linewidth for a collection of QBs seems very hard to achieve by any means. Even the size selection of vapor grown clusters does not seem to achieve this objective, as the selection acts on the cluster **mass** and not on the cluster three-dimensional **shape**, which determines the confinement energy. It therefore appears unlikely that the intrinsic linewidth of QBs in the 10 μeV range (Fig. 10) can be put to work in QB lasers.

The second requirement cannot be satisfied on a "first-order" analysis of energy relaxation in a fully-quantized system like a QB: due to the discreteness of energy levels, it is not possible to conserve energy and momentum in LO or LA phonon-induced transitions, as soon as the lateral box-size is below 1000 Å or 300 Å in the cases of electron or exciton relaxation respectively[29,30]. One then expects carrier accumulation in excited states, therefore broadening the emission band and gain curve and diminishing the overall quantum efficiency if some competing nonradiative recombination channels are present[29] (Fig. 11). Experimentally, the older attempts indeed show (i a decline of quantum efficiency with box sizes, however quite often
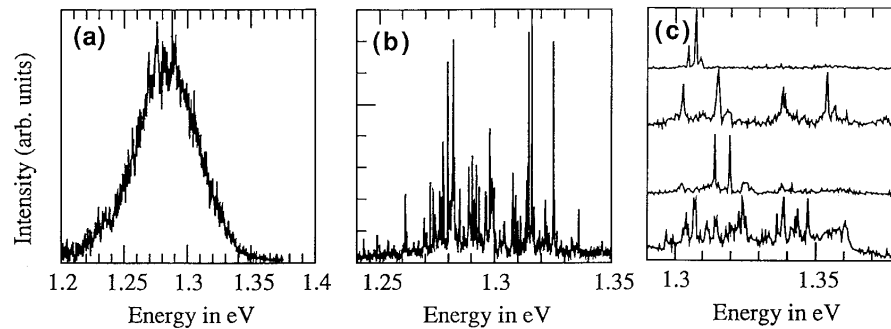
Figure 10. Photoluminescence spectra from mesa-shaped ensembles of InAs quantum dots imbedded in GaAs (a): 5000 nm diameter mesa, containing $\approx$ 8000 dots; (b) 500 nm mesa; (c) upper three curves: 200 nm mesas, containing each $\approx$ 15 dots; lower curve: summation of 20 spectra from different mesas [From J.Y. Marzin et al.[34]].

assigned to fabrication-induced damage. Also, the operation of a QW laser placed in quantizing perpendicular magnetic fields did show an increase of the threshold current[31], well compatible with the phonon relaxation bottleneck model[29] and the observed slowing down of e-e collision- induced relaxation in quantizing magnetic fields[32].

In direct-growth samples, both cases of efficient multiple sharp-line and single line emission have been observed on **single QBs** with fast onset times[20,33−35]. Such efficient carrier relaxation might be due to higher order effects (like Auger recombination[36] or multi-phonon scattering[37]. While the later mechanism seems to only yield efficient relaxation for narrow ranges of energy around the LO phonon energy, the Auger recombination mechanism seems particularly efficient, even at carrier densities in the few 10^{15} cm^{-3} range in the confining material. One might wonder if such densities are existing in the confining material, and the answer is yes, and certainly way beyond. Considering 100 Å×100 Å boxes with a 200 Å center-to-center separation (i.e. a box density of 2.5 1011 cm^{-2}) and a 1000 Å thick confining layer, the latter have equivalent electron and hole densities of 5.10^{12} and 7.10^{13} cm^{-2} at 300 K respectively. To ensure inversion, the quasi-Fermi levels are above the confined electron and hole levels respectively. Assuming a 100 meV confinement energy for each type of carrier (an optimistic value) and a Boltzmann factor for occupancy of confining layer states (an optimistic value if the quasi-Fermi level is above the confinement levels) of exp - $100/25 \approx 1/40$, one finds that $\approx 10^{11}$ electrons and 1.8 10^{12} hole levels are populated in the confining layers ! (of course

a precise evaluation ought to ensure some local charge neutrality in a self-consistent manner). This means that thermal excitation at room- temperature should create enough carriers in the confining layer to efficiently relax QB carriers by the Auger mechanism[36]. However, these thermally-excited carriers are created by a leakage current which is 50 Å cm^{-2} if the carrier density is 10^{12} cm^{-2}, in fact much larger than the current determined from gain requirements alone. It will dominate the total threshold current, bringing it back to values typical of QW lasers.

Taking an opposite approach, one can try to take advantage of the relaxation bottleneck in conditions under which it exists. It can be put to good use for intersubband- based devices such as the quantum cascade laser or IR detectors as they are often limited by fast LO-phonon-induced decay of excited QW states[38] (Fig. 11). For such devices, positive action of 3D quantization occurs as soon as phonon relaxation is hindered, i.e. at box sizes in the 700 Å range. They should therefore be quite easier to manufacture than electronically-quantized QBs. Another application of "large" boxes is through their action as localized radiative centers imbedded in non-radiative materials such as highly dislocated ones. The fast capture of carriers into the radiative boxes would prevent carriers to diffuse to the non-radiative centers, and therefore would lead to high-efficiency materials.

While the bulk of the above discussion applies to III-V imbedded QBs like in the GaAs/GaAlAs system, other materials systems can behave quite differently. Solution- grown, passivated CdS nanospheres exhibit excellent room-temperature luminescence based on efficient energy relaxation through surface states[39]. Mn-

(a)

capture

non
radiative
channels

slowed relaxation

~10 kT

radiative channels

$\Delta_{l,m,n}=0$

kT

(b)

Radiative efficiency

10^{0}
10^{-1}
10^{-2}
10^{-3}
10^{-4}
10^{-5}

SQUARE BOX

L

4K

10 L

pseudo wire

— 100 Å GaAs
— 100 Å InGaAs

20   50   100 200   500

Lateral box size (nm)

(c)

T_{blip}/T_{blip}

2
1
2
1

(a)

PC detector

$\lambda = 50$ um

(b)

PV detector
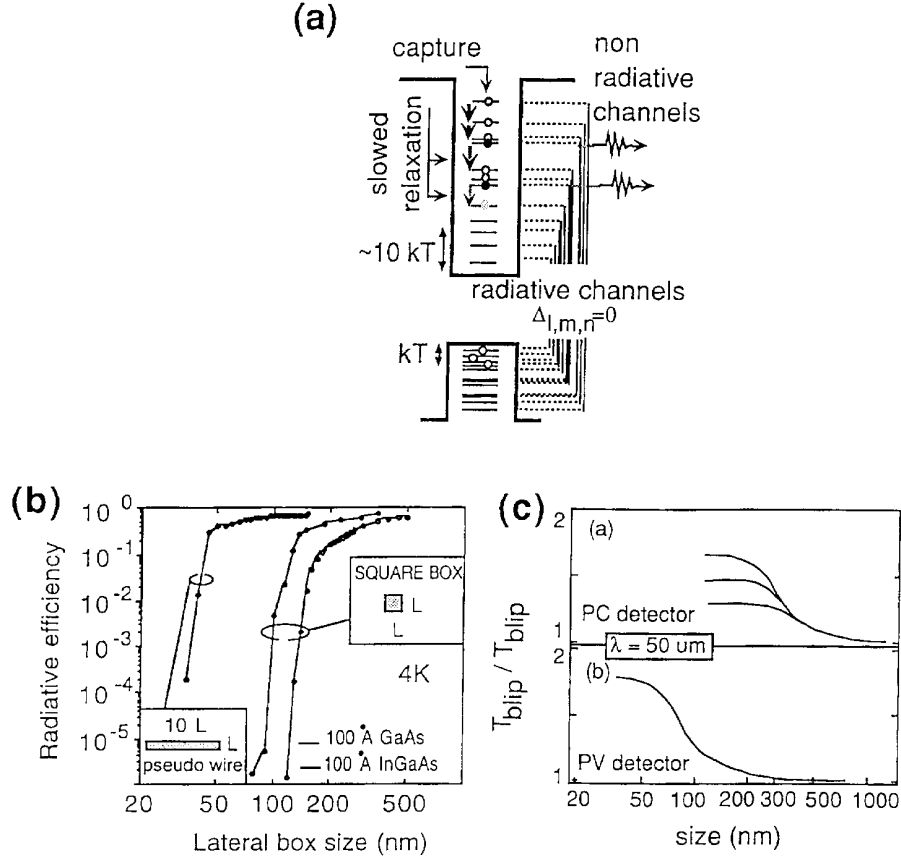
20   50 100 200 300 500 1000

size (nm)

Figure 11. Schematics of the phonon relaxation bottleneck (a) in Quantum Wire and Quantum Boxes and its impact on their luminescence quantum efficiency (b) and on BLIP temperature of infrared photoconductive (PC) or photovoltaic (PV) intersubband QW detectors (c), (H. Benisty and C. Weisbuch[38]).

doped CdSe nanospheres evidence a marked increase in spontaneous emission rate as well as an efficient conduction-electron to localized-electron energy transfer mechanism[40].

III.2 Confined photon structures

III.2.1 The basic phenomenon: interference enhancement and control of spontaneous emission

Photon confined structures come in two related families: microcavities and photonic bandgap (PBG) materials. They however originate from the same phenomenon, that of amplitude build-up due to multiple, in-phase reflections of optical waves. What differs is the fact that these reflections either occur on **localized mirrors** in microcavities or on **distributed interfaces** acting as light scatterers in photonic bandgap (PBG) materials. (For the sake of completeness, it can be added that similar build-up can also occur in disor-

dered dielectric structures, very similar to electron localization in disordered potentials). As it can be shown that both types of structures lead to a similar degree of light localization[41], we will describe here the simpler case of microcavity structures. Let us start with a major difference with electron confinement, that of amplitude concentration: consider a planar Fabry-Perot cavity, with mirror transmission and reflectivity coefficients T and R respectively, with mirror distance L leading to a resonant vertically propagating mode with eigenfrequency $\nu_0 = c/2L$. That mode amplitude, i.e. the ratio of the inside built-up wave intensity to an incoming wave, is $4/(1-R)$, while that of the perpendicular non-resonant modes (i.e. at other frequencies) is suppressed by a factor $(1-R)$. If one were to evaluate field amplitudes at a given frequency but at different incoming angles θ, for which the resonant mode frequency would be $\nu_0(cos\theta)^{-1}$, the same suppression factor $(1-R)$ would be obtained for non- resonant modes, i.e. at angles different from the normal: the unique feature of

microcavities (and PBG materials) is therefore to concentrate the field intensity into the resonant mode by as much as they suppressed it in non-resonant modes. As this is also true for the vacuum-field fluctuations, this means that spontaneous emission can be preferentially emitted in one resonant mode while suppressed in other modes. The detailed analysis[42,43] leads to an increased E-field intensity of allowed mode by the quality factor Q, an allowed mode width of $\Delta\omega/\omega \sim Q^{-1}$, and rejection of the mode amplitudes at other frequencies by a factor Q^{-1}.

This effects allows the control of spontaneous emission, as the overall spontaneous lifetime will almost be unchanged[43]. It is of paramount importance that the resonant mode is enhanced as otherwise cavity discretization of optical modes would certainly select modes, but at the same time would generate light in these modes at unuseful low rates if the lifetime were just proportional to the number of active modes. This is a major difference with electron quantization where the reduction in available states (due to the Pauli exclusion principle) leads to single QB systems which have very little action on a standard optical beam (see part 3.3 for a more detailed comparison between electron and photon mode quantization).

[In the field of atomic physics it is often evaluated that the spontaneous emission rate can be suppressed, or strongly increased by a factor $\lambda^3 Q/8\pi V$ (where V is the cavity volume), depending on the overlap of the cavity resonance with the atomic transition[22,42]. This only occurs when the atomic linewidth is narrower than the cavity linewidth, which is usually not the case in semiconductors where the effective linewidth is kT. Then, in solid-state microcavities, the modifications of spontaneous lifetime are quite small[42,43].

III.2.2 The weak-coupling microcavity: LEDs and lasers

The selection of photon modes has many effects, which have already been put to good use: multiple reflections lead to build-up of light emission in a given direction, thus leading to directionality. This sole effect could have dramatic impact in LEDs and displays in that it solves the major difficulty in light extraction from solids: usually, internal Lambertian sources have an external efficiency in the percent range in useful outside angles due to the refraction factor at the solid-air interface ($n_2/n_1 \approx 3.5$). In microcavities, the multiple reflections select an escape cone which is much smaller that the 2π angle of Lambertian source (of the order of $\pi(1 - R)$, where R is the mirror reflectivity) leading to small outside emission angle, even when taking into account the beam widening due to the refractive index change[42,43]. Another useful effect is that of spectral narrowing: due to the spectral width of allowed photon modes, light within a photon mode can be quite narrower than the usual thermally-broadened emission. This has been put to good use to increase by a factor of three the transmission capacity of optical fiber systems where chromatic dispersion is the limiting factor[44].

III.2.3 Microcavity LEDs

One should be cautious: the above effects evidence optical mode reinforcements and selection. They don't show that there is an increase in light extraction efficiency in the resonant mode. Experimental proofs require calibrated absolute measurements. On the theory and modeling side, one has to ascertain that competing spontaneous emission channels have been suppressed, or at least greatly diminished.

The factor of merit describing the control of spontaneous emission into a desired mode is called the spontaneous emission factor β defined by

$$\beta = \frac{\text{spont. emission in desired mode}}{\text{spont. emission in all modes}} \quad (12)$$

To bring β close to unity in a vertical planar cavity geometry amounts to a fight against recombination into various competing modes (Fig. 12b):

- Into the leaky modes of the Bragg reflectors, due to the fact that Bragg mirrors are efficient up to a critical angle θ_c such as $cos^{-1} \theta_c = (n_2 - n_1)/n$, where n_2, n_1 and n are the refractive indices of the layer materials and their average respectively. Beyond that angle, the Bragg mirror almost act as an homogeneous dielectric medium with average index n.

- Into the guided modes, which are particularly important in the electron confining layers, which have a smaller bandgap and therefore an index of refraction higher than the surrounding layers.
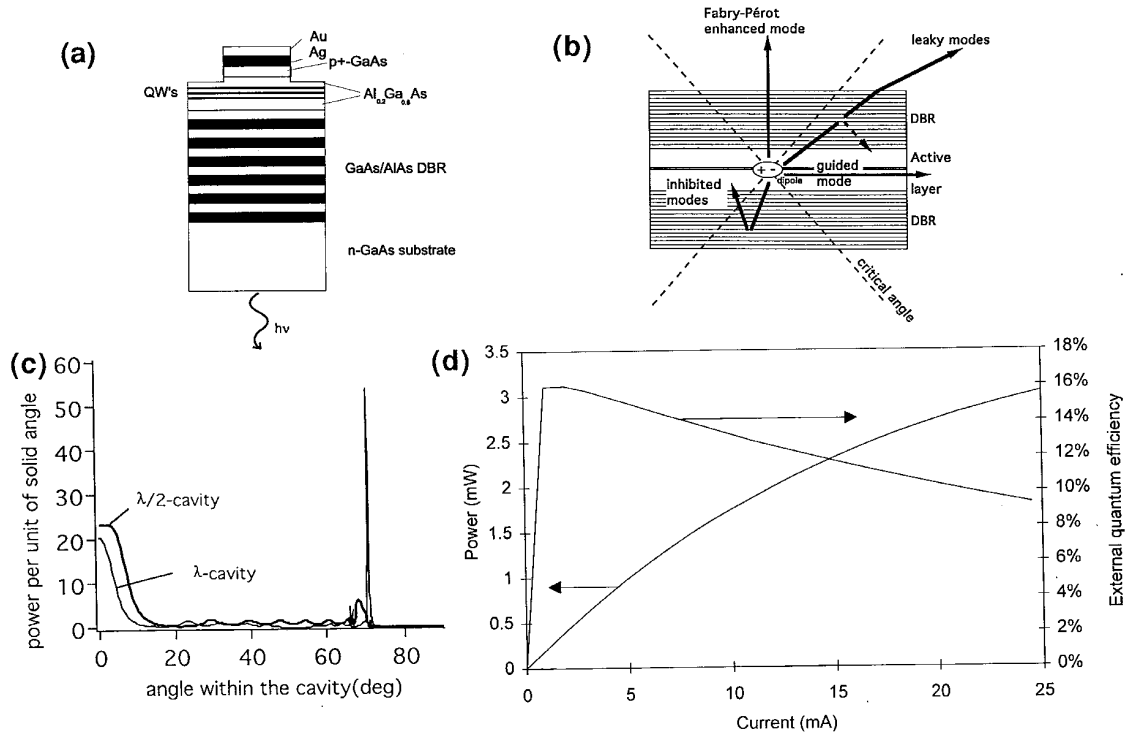
Figure 12. Schematics of the operation of a high-efficiency LED: (a) LED structure; (b) outline of the various competing modes; (c) calculated emission diagram for $\lambda/2$ or λ cavities: note the much larger guided-mode emission for the λ cavity for which the overlap of the guided-mode with the quantum wells is significantly increased as the asymetry of the mirrors plays a lesser role; (d) emitted power and efficiency [From Blondelle J.[47]].

- Into the oblique modes, whenever the emission spectrum is broader than the cavity linewidth, given by $\Delta\lambda = \lambda/2F$, where F is the cavity finesse ($F = \pi/1 - R$). As mentioned earlier, the planar cavity is a 2D system for photon modes, and emission at wavelengths shorter than that of the cavity fundamental vertical mode ($\lambda_0 = 2L/m$, m being the order of the mode) occur on resonant oblique modes of wavelength $\lambda = \lambda_0 cos\theta$. In that case what the cavity does is to redistribute the spontaneously emitted light into cones of monochromatic light instead of the quasi-isotropic distribution of light intensity and wavelengths from random dipoles in free space. This property can be used to extract a given wavelength from a broadband source, by angular selection. This is what is being achieved with organic dye emitters[46]: by using spatially-varying cavities with three different thicknesses, the light at the three basic colors is concentrated in the forward viewing direction to achieve a color display from a single light-emitting molecule.

The search for high efficiency emission is well un-

der way[45−47]. The best results so far are those obtained from university of Gent[47] where an extraction efficiency of 16% is achieved in the planar geometry shown in Fig. 12a. The modellization of spontaneous emission in the various modes is shown in Fig. 12b. The use of a metallic mirror on one side, also used as an electrode, suppresses the "leaky" modes in one half- space. In addition, the high index of the metal mirror "repells" the in-plane guided mode away from the active region. Hence, the vertical emission mode has been enhanced at the expense of the guided and leaky modes. The Bragg mirror reflectivity is adjusted to 70%. This value shows that optimal outcoupling in LEDs is obtained for structure designs very far from that of VCSELs. A bad laser does not make a good LED ! The theoretical limit to efficiency is in the 30% range. Improvement could still be made by using a lower-loss metal and by using a Bragg mirror with fewer "leaky" modes, i.e. with an higher index difference such as $Al_xO_y^{[8]}$.

Only a few studies have been so far devoted to the improvement of EL displays by spontaneous emission control[48], beyond the use of a back mirror reflecting the light emitted backwards into the viewing an-
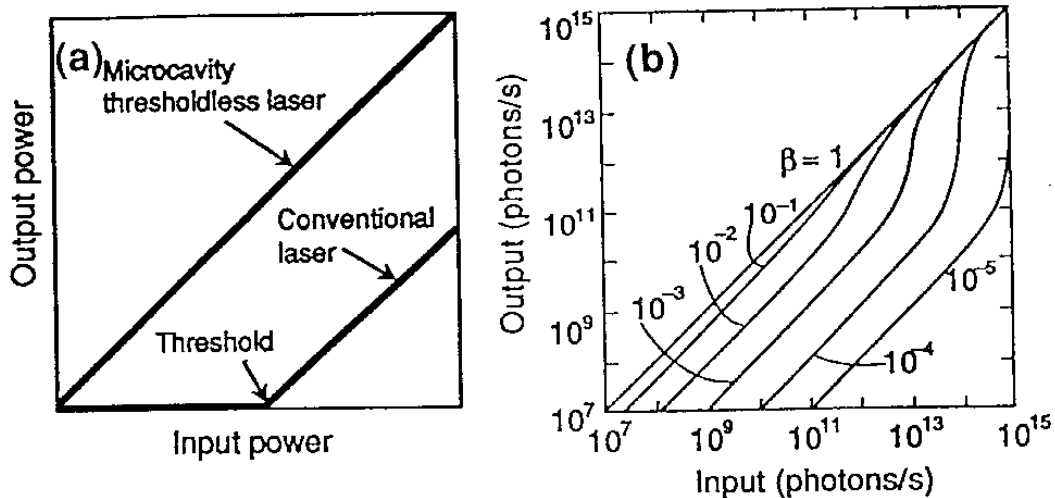
Figure 13. Schematics of the characteristic emission curve of a thresholdless $\beta = 1$ laser as opposed to a conventional laser (a) and its modelisation as a function of the value of β, spontaneous emission factor (b) (From Yokoyama[42]).

gle. One of the difficulties is the electrical insulation requirement which leads to rather thick cavities using existing technologies. Neverless, there certainly is room for improvement as present-day extraction efficiency is in the 10% range.

III.2.4 Microcavity lasers

In the laser field, the control of the spontaneous emission, as characterized by the spontaneous emission factor β (ratio of the intensity emitted in the laser mode to that emitted in all modes) can have dramatic effects: if $\beta = 1$, the emission quantum efficiency in the unique photon mode does not change when switching from spontaneous to stimulated emission with photon number. One reaches a "thresholdless" laser operation[42,43,49]. What is being acted on is the τ factor in equation (11), which is being divided into $\beta\tau^{-1}$ and $(1-\beta)\tau^{-1}$, representing the emission rates into and out of the laser mode. In such an analysis, only $(1-\beta)\tau^{-1}$ is a loss. The rate equation modellization then leads to the characteristic curves shown in Fig. 13. Compare this powerful leverage on laser operation with that due to QBs, which mainly modifies the differential gain. In addition, photon emission becomes fully deterministic, leading to the generation of photon-number squeezed states which should allow better signal-to-noise ratios in optical communications[23,51].

The $\beta = 1$ limit is difficult to achieve in **planar microcavities** due to both the existence of "leaky"

and guided modes in such 2D structures, and to the broad emission spectrum[50,52] (Fig. 14). One requires OD microcavities or PBG materials in order to suppress these modes and reach $\beta = 1$. This is the major present challenge in the field.

III.2.5 The strong light-matter interaction: cavity-polaritons

When placing quantum-wells inside a planar microcavity a very simple and unique situation develops: both quantum well excitons and resonant photon modes span two-dimensional states spaces, but due to the translational symmetry of the system the transverse wavevector is conserved in the optical transition (Fig. 15). Therefore, only the states having the same
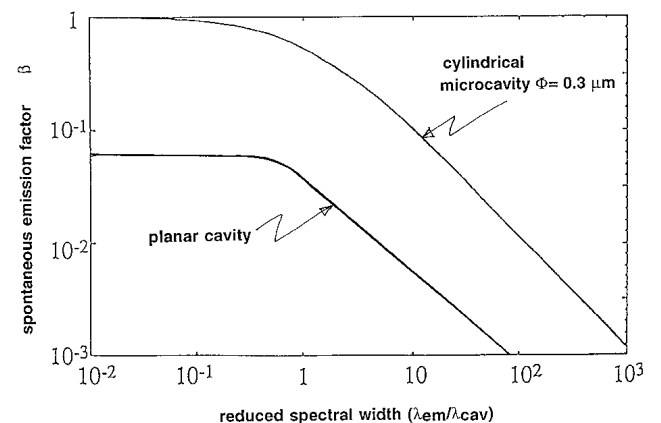

Figure 14. Spontaneous emission factor β of for a planar Bragg-mirror cavity and for a cylindrical microcavity, as a function of the emission linewidth (from Bjork et al.[35]).
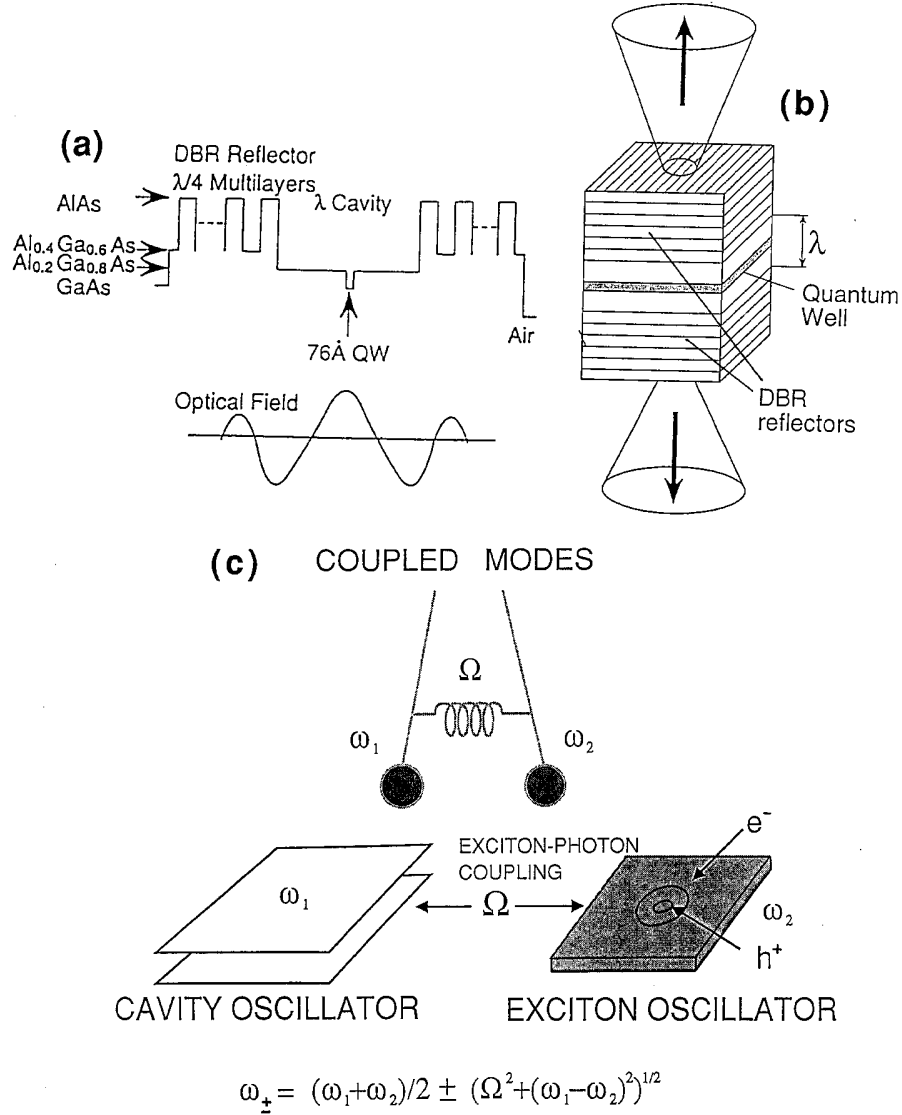
Figure 15. Strong-coupling in semiconductor microcavities: (a) spatial variation of the conduction band minimum and of the optical field through the structure; (b) schematics of the structure (c) representation of the coupled exciton and photon modes as oscillators.

wavevector K in the 2D dispersion curves interact . For each K-value, we have two oscillators (one mechanical, the exciton, one electromagnetic, the photon) which are coupled through the exciton-photon interaction. This is reminiscent of the exciton-polariton phenomenon in bulk semiconductors, and likewise, coupled-mode behaviour develops if the coupling strength is larger than dissipating mechanisms[53]. Let us discuss the figures: at room temperature, the exciton scattering time (due to L0 phonons) is in the 5 meV range, i.e. 1 ps. For a 1 μm-long, 99.7 % reflectivity microcavity, the photon lifetime is also 1 ps. The coupling strength, represented by the Rabi frequency of the exciton dipole in the vacuum-field, is given by $\hbar\Omega = \mathbf{p}.\mathbf{E}$, where $\mathbf{p}$ is given

by the QW exciton oscillator strength $f \approx 4.10^{12}$ cm^{-2} and $\mathbf{E}$ by $(\hbar\omega/2\epsilon_0\epsilon V)^{1/2}$. With 3 QWs in the cavity, then $\hbar\Omega \simeq 5$ meV, sufficient to overcome photon loss and exciton scattering.

The remarkable enhancement of exciton binding energy and oscillator strength in QWs allows the occurence of this strong-coupling phenomenon up to room- temperature[54].

The luminescent properties of such light-matter strongly-coupled systems raise new questions: what are the light-emission mechanisms ? Are the dynamical processes modified ? Are such strongly-coupled systems interesting for new applications, such as thresholdless lasers or exciton-based lasers ? etc... Although a com-

plete answer to these questions is not possible yet, we can describe some interesting results.

A complete description of the luminescence of the resonant coupled-excitations could be complicated: one has both to calculate relaxation effects and emission properties of each mode. In atomic physics, the situation is much simpler as one deals with isolated transitions and one can directly calculate the atomic dipole radiation in a strong-coupling regime[55]. Here, we will rather use the very powerful formalism developped for excitonic-polaritons in bulk semiconductors[56−60]. In that description, one considers that polaritons reach a quasi-equilibrium distribution among allowable states. Knowing that distribution, light emission out of the crystal is then a matter of polariton propagation to the surface and their transfer out of the crystal as photons. We believe that this picture is correct for cavity polaritons but there the situation is quite simplified compared to the bulk situation: first, this is a 2D system acting as a set of plane-localized dipole emitters. There is no propagation phenomenon to the surface like in 3D. Second, excitations have no momentum perpendicular to the QW plane. Therefore, there is a one-to-one correspondance between a cavity polariton and an outside photon with an equal transverse-momentum, whereas for the bulk material a measured (outside) photon corresponds to inside polaritons with various momenta which have been scattered out in the right direction. Therefore, in 2D microcavities the angle-resolved emission $I(E, \theta)$ intensity is proportional to the product of the absorption coefficient [proportional to $\rho(E)$ $T(E, \theta)$ where $\rho(E)$ is the density of states, a constant in 2D, and $T(E, \theta)$ the transmission coefficient at energy E and in direction θ] by an occupancy factor[54] (Fig. 16a). Conversely, observing $I(E, \theta)$ as a function of θ allows to determine the peaks in $T(E, \theta)$, directly linked to the energy levels of cavity polaritons. Doing so, we directly map the cavity polariton dispersion curve[61] (figure 16c).

The strong-coupling regime creates an ultrafast radiative recombination channel: the usual weak-coupling emission rate is given by Fermi's golden rule (which can be expressed as $\Omega^2 \rho(\omega)$, Ω being the Rabi frequency and $\rho(\omega)$ the density of continuum photon states to which

the electronic level is coupled[22]. Lifetimes are then in the nanosecond range. In the case of strong coupling, the radiative lifetime of coupled-mode excitations is the photon lifetime in the cavity, in the ps range. Indeed, under resonant excitation, the Rabi oscillation is observed with a decay of the excited material in the ps range. In that case, as excitations cannot relax to any other quantum state, a $\beta = 1$ laser is achieved[62,63]. However, this is a rather "academic" situation as excitons are created non-resonantly in electrically-injected devices . When using a non-resonant optical excitation, the decay time of the microcavity falls back in the nanosecond range[64]. This is due to the fact that the fast-recombining coupled-modes are fed from a wide portion of the phase-space of uncoupled, large-wavevector thermal excitons with a relaxation time in the ns range due to acoustical phonons.

It therefore remains to be seen whether this unique strongly-coupled optical "material" can lead to applications such as thresholdless lasers or electro-optical, non- linear optical devices. One of the more fascinating recent proposal is the use of microcavities as the basic quantum gates to be used in quantum computing systems[65].

III.3 A comparison between the electron and photon confinement schemes

It is useful to compare in a basic manner the two approaches of confinement. Let us consider a single-electron quantum-box, interacting with a continuum of blackbody photon modes or with a standard 1mW light beam, and an optical microcavity, of size $\approx (\lambda/2n)^3$ interacting with optically active medium located within the microcavity. In the first case, the electron-photon interaction of the single electron states are unmodified when compared to bulk material, at least to first-order: the lifetime and oscillator strength are unchanged. However, the optical beam has not enough interaction with the electronic system: it can only generate $\approx 10^9$ (spontaneous rate) $-10^{10,11}$ (stimulated rate) transitions per second, not enough to efficiently control or generate a sizeable optical beam. Moreover, the confinement factor, due to the overlap of the optical beam with the quantum box, is small, fundamentally due to the difference in wavelengths between the electron and photon. In the second case the lifetime of the
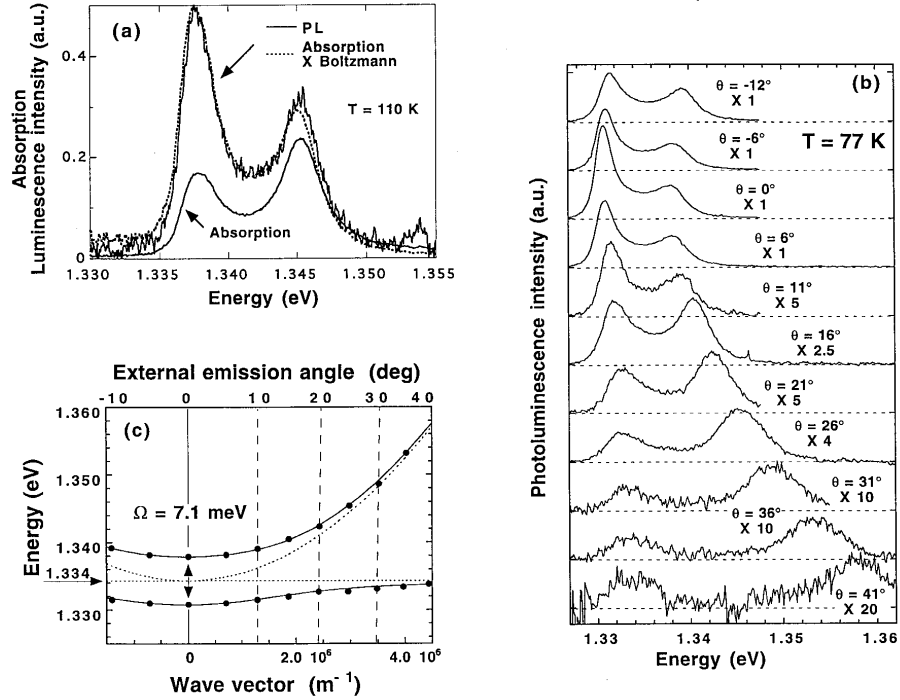
Figure 16. (a) Luminescence of cavity-polaritons at $\approx$ 100 K and its fit to a curve determined by the product of the absorption coefficient (measured as 1-T-R [T and R transmission and reflectivity of the structure respectively] times a Boltzmann factor); (b) Angular-resolved photoluminescence; (c) Dispersion curve (full line, theory; full points: experiment) of the cavity-polaritons (E vs. in-plane momentum K) as deduced from the peak positions of luminescence as a function of angle θ, which are given by the resonances of $T_i(E, \theta)$, themselves equal to an excellent approximation to the E_i values for a given angle θ. The dashed curves represent the uncoupled photon and exciton dispersion curves (bottom) [From Houdré et al.[54]].

electronic excitations is almost unchanged, as well as its coupling to the optical fields: the resonance effect of the cavity increased as much the resonant electric field as it decreased all other fields. The cavity acted as a concentrator of optical fields into a single optical mode. However, in this case, the active material volume ($\approx (\lambda/2n)^3$) is such that it can contain enough quantum states ($> 10^6$) in bulk, or multi-QWs, QWWs, QBs, so that they can control or generate a sizeable optical beam ($10^{15} - 10^{18}$ transitions per second). In addition, photon spontaneous emission occurs selectively in the cavity mode, which is not achieved for QBs coupled to a continuum of photon modes.

It can be said that the situations of electron or photon confinements are not symetrical: whereas both bring sharper optical features, the photon confinement scheme adds mode selectivity and a single microcavity handles enough power to achieve a useable device, whereas the electron confinement scheme requires a large number of quantum boxes to achieve sizeable effects. This difference can be traced to the Boson nature of photons, which allows many photons in a single op-

tical mode, whereas the Fermion nature of the electron allows only one electron in a given quantum state (a single electron mode) in a quantum box.

IV. Conclusion

There is still room for major improvements in ligth-emitting devices based on novel physics. The two fields of electron and photon confinement are well alive and bringing us continuously new results, challenges and even surprises. The former is making spectacular progress fabrication-wise. While I am personally wondering about the real impact (and need) of QB lasers, the possibility of intersubband, relaxation bottleneck-based devices appears both more useful and easier to reach. Photon confinement schemes are still very young but appear to give a very powerful leverage on the photon-matter interaction. They could have a major impact on LEDs and displays. The strong coupling case is still to be evaluated for device action, and fabrication techniques for 3D microcavities or PBG materials are to be developed. Whereas the bulk of activity is devoted to lasers and LEDs, other optical and optoelectronic

devices should not be left aside.

Acknowledgments

It is a pleasure to thank all those with whom I collaborated along the years in the various aspects of light-matter interaction and laser devices. In 1979-1981, I had the good fortune to be at Bell Laboratories, working with Ray Dingle primarily, and interacting at various degrees with A. Cho, W. Tsang, A. Gossard, P. Petroff, H. Stormer, C. Shank, J. Hegarty, M. Sturge, R. Fork and many others. In Thomson during 1983-1992, the work on quantum well lasers was mainly carried out by (then) graduate student J. Nagle, with collaborations with J. P. Hirtz, M. Razeghi, P. Hirtz, B. De Cremoux, while the work on quantum dots was carried out with J. Nagle, H. Benisty and E. Bockenhoff, with collaboration with C.M. Sotomayor-Torres from the University of Glasgow. The work on the strong coupling in microcavities was started as an NTT chair visiting professor at the University of Tokyo, in Professor Y. Arakawa's laboratory, and also benefited from the collaboration of A. Ishikawa and M. Nishioka. The recent work on microcavities is carried out in the Ecole Polytechnique Federale de Lausanne with R. Houdré, R. Stanley, U. Oesterle, P. Pellandini, M. Ilegems. The present work on photonic bandgap materials and microcavities at Ecole Polytechnique, Palaiseau, is done with H. Benisty.

References

1. W.N. Carr, Infrared Phys. **6**, 1 (1966).

2. G. Craford, IEEE circuits and devices mag. **8** (Sept. 1992) 24; G. Craford and F. M. Steranka, *Light Emitting Diodes*, in Encyclopedia of Applied Physics, vol. **8** (VCH publishers, 1994); Werner K., IEEE Spectrum July 1994, p. 30.

3. For a general reference in the field, see e.g. C. Weisbuch and B. Vinter, *Quantum Semiconductor Structures*, (Academic, Boston, 1991).

4. E. Burstein and C. Weisbuch, *Confined Electrons and Photons: New Physics and Applications*, (Plenum, New-York, 1995).

5. see e.g. A. Yariv, *Quantum Electronics*, 3rd ed. (Wiley, New-York, 1989); P.W. Milonni and J.H. Eberly, *Lasers* (Wiley, New-York, 1988); B.E.A. Saleh and M.C. Teich, *Fundamentals of Photonics* (Wiley, New-York, 1991).

6. H.C. Casey and M.B. Panish M.B., *Heterostructure Lasers*, vol. A, (Academic, New-York, 1978).

7. J.P. Van der Ziel and M. Ilegems, Appl. Optics **14**, 2627 (1975). R. S. Geels, J.W. Corzine and L.A. Coldren, IEEE J. Quantum Electr. QE-**27**, 1359 (1991).

8. D.L. Huffaker, C.C. Lin, J. Shin and D. G. Deppe, Appl. Phys. Lett. **66**, 3096 (1995).

9. G.M. Yang, M.H. Mac Dougal and P.D. Dapkus, Electronics Lett. **31**, 886 (1995).

10. See the discussion in the remarkable historical comment by C. H. Henry, The Origin of Quantum Wells and the Quantum Well Laser in Quantum Well Lasers, Zory P.S. ed., (Academic, Boston, 1993).

11. P. L. Derry et al., Appl. Phys. Lett. **50**, 1773 (1987); T.R. Chen et al., Appl. Phys. Lett. **56**, 1002 (1990).

12. J. Nagle, S. D. Hersee, M. Krakowski, T. Weil and C. Weisbuch, Appl. Phys. Lett. **49**, 1325 (1986); J. Nagle and C. Weisbuch, J. of Luminescence **40** & **41**, 713 (1988); J. Nagle and C. Weisbuch, Inst. Phys. Conf. series no. **91**, 617 (1988).

13. T. Takagi et al., IEEE J. Quantum Electronics **QE-27**, 1511 (1991).

14. S. D. Lester, S. A. Ponce, M. G. Craford and D. A. Steigerwald, Appl. Phys. Lett. **66**, 1249 (1995).

15. see e.g. S. Strite, *The III-V Nitride Semiconductor Blue Light Emission: Recent Progress and a Critical Evaluation of their Potential in Comparison to the Zn Se Based II-VI Semiconductors* in Festköperprobleme 32, Vieweg (1994).

16. J. Faist, C. Capasso, Appl. Phys. Lett.**66**, 538 (1995).

17. N. W. Carlsson, *Monolithic Diode-Laser Arrays* (Springer, Berlin, 1994).

18. R. L. Byer, Science **239**, 742 (1988).

19. A.F.J. Levi et al., Electronics Lett. **28**, 1010 (1992).

20. J. Y. Marzin, A. Izrael and L. Birotheau, Solid-State El. **37**, 1091 (1994).

21. For a recent review see R. E. Slusher and C. Weisbuch, Solid State Commun. **92**, 149 (1994).

22. See P. R. Berman ed., *Cavity quantum electrodynamics*, (Academic, Boston, 1994). As an excellent short introduction, see S. Haroche and D. Kleppner, Physics Today, **42**, 24 (1989).

23. See, e.g., E. Yablonovitch, J. Opt. Soc. Am. **B 10**, 283 (1993), and the other papers in this special issue of the J. Opt. Soc. Am. on Photonic Bandgap Materials.

24. See, e.g, the special issue of the Journal of Modern Optics vol. 41, february 1994.

25. C.M. Soukoulis, *Photonic Band Gaps and Localization*, (Plenum, New-York, 1993).

26. J.D. Joannopoulos, R.D. Meade and J.N. Winn, *Photonic Crystals*, Princeton (University Press, Princeton, 1995).

27. T. Takagahara, Phys. Rev. **B47**, 4569 (1993); T. Takagahara, Phys. Rev. **B36**, 9293 (1987).

28. E. Hanamura, Phys. Rev. **B37**, 1273 (1988).

29. H. Benisty, C. M. Sotomayor-Torres and C. Weisbuch, Phys. Rev. **B44**, 10945 (1991).

30. U. Bockelmann and G. Bastard, Phys. Rev. **B42**, 8947 (1990); U. Bockelmann, Phys. Rev. **B48**, 17637 (1993) and contribution in ref. 4.

31. T.T.J.M. Berendschot et al., Appl. Phys. Lett. **54**, 1827 (1989).

32. J.B. Stark, W. H. Knox and D. S. Chemla, Phys. Rev. Lett. **68**, 380 (1992).

33. Y. Nagamune et al., Appl. Phys. Lett.**64**, 2495 (1994).

34. J.-Y Marzin et al., Phys. Rev. Lett. **73**, 716 (1994).

35. See also the contribution of J.-M. Gérard in ref. 4.

36. U. Bockelmann and T. Egeler, Phys. Rev. **B46**, 15574 (1992).

37. T. Inoshita and H. Sakaki, Phys. Rev. **B46**, 7260 (1992).

38. H. Benisty and C. Weisbuch, unpublished; H. Benisty, in Phonons in Semiconductors Nanostructures, J.P. Leburton et al. eds., Kluwer, Dordrecht, 1993, p. 447

39. M. G. Bawendi, P.J. Carroll, W.L. Wilson and L.E. Brus, J. Chem. Phys. **96**, 946 (1992); see also the contribution by Bawendi in ref. 4.

40. R.N. Bhagarva, et al., Phys. Rev. Lett. **72**, 416 (1994).

41. R. Stanley, R. Houdre, U. Oesterle, M. Ilegems and C. Weisbuch, Phys. Rev. **A 48**, 2246 (1993).

42. H. Yokoyama, Science **256**, 66 (1992); see also his contribution in ref. [4].

43. G. Bjork, S. Machida, Y. Yamamoto and K. Igeta, Phys. Rev. **A 44**, 669 (1991); G. Bjork, H. Heitmann and Y. Yamamoto, Phys. Rev. **A 47**, 4451 (1993); G. Bjork, IEEE J. Quantum El. **QE-30**, 2314 (1994).

44. N. E. J. Hunt, E. F. Schubert, R. F. Kopf, S. L. Sivco, A.Y. Cho and G. J. Zydzik, Appl. Phys. Lett. **63**, 2600 (1993).

45. E. F. Schubert et al., Science **265**, 943 (1994).

46. A. Dodabalapur et al., Appl. Phys. Lett. **64**, 2486 (1994).

47. De Neve et al., IEEE Photonics Technol. Lett. **7**, 287 (1995); J. Blondelle et al., Electronics Lett. **31**, 1286 (1995).

48. Van den Bossche et al., Proc. VIth Intal Workshop on Electroluminescence, V. P. Singh and J. C. Mc Clure eds., Cinco Punto Press (El Paso, Texas, 1992) p.393; R. H. Mauch, K. A. Neyts and H. W. Schock in *Electroluminescence*, S. Shionoya and H. Kobayashi eds. (Springer, Berlin, 1989) p. 291.

49. Y. Yamamoto and R. E. Slusher, Physics Today, June 1993, p. 66

50. T. Baba, T. Hamano, F. Koyama and K. Iga, IEEE J. Quantum Electron. **QE-27**, 1347 (1991).

51. Y. Yamamoto, S. Machida and W. H. Richardson, Science **255**, 1219 (1992).

52. See e.g. ref. G. Bjork, H. Heitmann and Y. Yamamoto, Phys. Rev. **B47**, 4451 (1993).

53. C. Weisbuch, M. Nishioka, A. Ishikawa and Y. Arakawa, Phys. Rev. Lett. **69**, 3314 (1992).

54. Houdré R. et al., Phys. Rev. **B49**, 16761 (1994).

55. See, e.g. J. J. Childs, K. An, R. R. Dasari and M. S. Feld in Advances in *Molecular and Atomic Physics*, suppl. 2, P.R. Berman ed., (Academic Press, Boston, 1993).

56. Y. Toyozawa, Prog. Theor. Phys. Suppl. **12**, 111 (1959).

57. J. J. Hopfield, Proc. Int. Conf. on the Physics of Semiconductors, Kyoto (1966), J. Phys. Soc. Jpn. **21 suppl.**, 77 (1966).

58. D. D. Sell, S. E. Stokowski, R. Dingle and J. V. Di Lorenzo, Phys. Rev., **B7**, 4568 (1973).

59. H. G. Sumi, J. Phys. Soc. Jpn. **41**, 526 (1976).

60. C. Weisbuch and R. G. Ulbrich, J. Lumin **18/19**, 27 (1978).

61. R. Houdré, R. Stanley, U. Oesterle, P. Pellandini, M. Ilegems and C. Weisbuch, Phys. Rev. Lett. **73**, 2043 (1994).

62. C. Weisbuch et al., 1992 Quantum Electronics and Lasers Conference, Anaheim, unpublished.

63. Y. Yamamoto et al., J. de Physique (France) **IV,C5**, 39 (1993).

64. T. B. Norris et al., Phys. Rev. **B50**, 14663 (1994).

65. Y. Yamamoto, Proceedings 1995 Les Houches Winterschool on Quantum Optics, unpublished; J. Jacobson et al., unpublished.